Supersolid and pair correlations of the extended Jaynes-Cummings-Hubbard model on triangular lattices

Lijuan Guo,[1] Sebastian Greschner,[2,*] Siyu Zhu,[1] and Wanzhou Zhang[1,3,†]

[1]*College of Physics and Optoelectronics, Taiyuan University of Technology, Taiyuan 030024, China*

[2]*Department of Quantum Matter Physics, University of Geneva, 1211 Geneva, Switzerland*

[3]*Key Lab of Advanced Transducers and Intelligent Control System of Ministry of Education, Taiyuan University of Technology, Taiyuan 030024, China*

(Received 7 June 2019; revised manuscript received 16 August 2019; published 18 September 2019)

We study the extended Jaynes-Cummings-Hubbard model on triangular cavity lattices and zigzag ladders. By using density-matrix renormalization-group methods, we observe various types of solids with different density patterns and find evidence for light supersolids, which exist in extended regions of the phase diagram of the zigzag ladder. Furthermore, we observe strong pair correlations in the supersolid phase due to the interplay between the atoms in the cavities and atom-photon interaction. By means of cluster mean-field simulations and a scaling of the cluster size extending our analysis to two-dimensional triangular lattices, we present evidence for the emergence of a light supersolid in this case also.

DOI: 10.1103/PhysRevA.100.033614

I. INTRODUCTION

Searching for novel supersolids (SS) and exploring their nature is an interesting topic in the field of condensed-matter physics [1–4]. The controllable ultracold-atom system provides a pristine and convenient platform to realize such tasks [5,6] with multicomponent systems of ultracold atoms being possible candidates to host the SS phase [7–10]. In particular, Bose-Einstein condensates in cavities have allowed for the successful observation of supersolids in experiments [11,12]. Recently, supersolid properties have been found also in systems of dipolar quantum droplets [13,14].

The Jaynes-Cummings-Hubbard (JCH) model, a combination of the Jaynes-Cummings (JC) model [15,16] of coupled cavities where each cavity contains a two-level atom, is an interesting variant of cavity coupled quantum systems. Experimentally, the JCH model can be realized by a coupled transmission-line resonator [17] or trapped ions [18]. Analytically, the mean-field (MF) theory [19,20], the Ginzburg-Landau theory [21], the strong-coupling random-phase approximation method [22], and the Green-function method [23] are all used to study the properties of the JCH model. Furthermore, the correlation and critical exponents of the JCH model can be obtained by many reliable numerical methods, such as the density-matrix renormalization-group algorithm (DMRG) [24,25] and the quantum Monte Carlo (QMC) method [26,27].

Moreover, several interesting topics concerning the JCH model have been studied, which include fractional quantum Hall physics [28], quantum transport [29], quantum-state transmission [30], on-site disorder [20,31], three-body interactions [32], and the interesting quantum phase transition between the superfluid (SF) phase and the Mott-insulator (MI) phase [16]. All of these previous works ignored the interaction between atoms. Until recently, the light superradiant solid was found in the Dicke model of a cavity modeled by quantum electrodynamics coupled with a one-dimensional Rydberg lattice [33]. However, since the photon hopping between each cavity was not considered, it remains unclear whether or not the photon hopping will induce the supersolid phase, where the solid order and superfluid order coexist simultaneously and the solid could also be called density wave (DW). In Ref. [34] a light supersolid in the extended JCH model on the square lattices was found by MF methods. It is still necessary to study the JCH model on other lattices by more reliable methods.

In the limit of a dominant atom-photon coupling, as will be discussed below, the extended JCH model may be mapped on a Bose-Hubbard (BH) model. Since, for the extended BH model, a broad regime of supersolid phases was found, in particular, on triangular lattices [35–37], it is interesting to study the extended JCH model on the triangular cavity lattices away from this limit and check whether additional SS exists in the phase diagram. Here the light supersolid phase may be stabilized by an order-by-disorder mechanism as discussed in Refs. [35–37].

In this work, we study the extended JCH model on the triangular zigzag ladders and lattices in the low filling regime by means of arguments in limiting cases and detailed numerical DMRG and cluster mean-field (CMF) simulations. For the quasi-one-dimensional zigzag ladder case we present example phase diagrams, which exhibit gapped DW phases at densities $\rho = 1/3,\ 1/2$, and $2/3$, as well as two extended regions of a pair-supersolid phase between the DW phases. We analyze properties of these phases and study the phase transitions to superfluid regions. We argue that the pairing inside the supersolid phase is a feature of the inherent quasi-1D geometry of the ladder system. In order to extend our study to 2D-triangular lattice geometries, we employ cluster mean-field simulations. We find a qualitatively similar phase

*Corresponding author: sebastian.greschner@unige.ch

†Corresponding author: zhangwanzhou@tyut.edu.cn

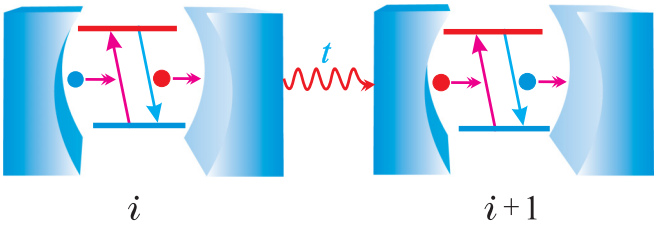

FIG. 1. Photon denoted by a red symbol is tunneling between two different cavities which are labeled by i and $i+1$, and t is the hopping strength. In each cavity, the atom has two energy levels which are labeled by two separated horizontal lines.

diagram with two gapped DW phases at $\rho = 1/3$ and $2/3$, as well as extended supersolid phases in between. In relation to previous results in a related bosonic model [35–37], for which we present an effective mapping in a limiting case, the emergence of these supersolid phases may be explained by an order-to-disorder–like mechanism. We present the qualitative general 2D phase diagram by MF simulations and show evidence at the stability of its main features, in particular of the SS and gapped phases by comparison to a simulation with various cluster sizes up to 12 sites. The experimental signatures of the SS phase are also shown by the momentum distribution and correlation.

The outline of this work is as follows. Section II shows the JCH model and the equivalence between the JCH model and the Bose-Hubbard model in the limit of dominant atom-photon coupling. Section III shows the results of the JCH model on the triangular zigzag ladder by the DMRG method. The phase diagram in the limit of vanishing intercavity hopping $t/U \to 0$ and the phase diagram containing the emergent paired-supersolid at finite $t/U \geqslant 0$ are shown in Secs. III A and III B. In Sec. III C, the pairing is verified by the quantities such as two-particle excitation binding energy, single and pairing particle correlation at various sizes of the systems, and explained in the Bose-Hubbard limit. In Sec. III D, the structure factor, the momentum distribution, and the fidelity susceptibility are shown to illustrate the supersolid phase and the Ising character of the transition between the P-SS phase to the SF phase. In Sec. IV, the impact of the transverse size of the SS phase is discussed via the three-leg triangular ladders. In Sec. V, for the JCH model on triangular lattices, the cluster MF method, the global phase diagram, and stability analysis of the supersolid are presented. Concluding comments are made in Sec. VI.

II. MODELS AND LIMIT OF ATOM-PHOTON COUPLING

Following Ref. [34], we consider a triangular lattice of coupled cavities as sketched in Fig. 1. On each cavity site i, the two-level atom with a ground state $|g\rangle$ and excited state $|e\rangle$ is contained. The on-site coupling between the photons and the atom on each site i can be described by the JC Hamiltonian H_i^{JC}

$$H_i^{\mathrm{JC}} = \omega n_i^a + \varepsilon n_i^\sigma + U(a_i^\dagger \sigma_i + a_i \sigma_i^\dagger), \tag{1}$$

where ω is the frequency of the mode of the photon creation and annihilation operators at lattice site i, ε is the transition frequency between two energy levels, and $n_i^a = a_i^\dagger a_i$ and $n_i^\sigma = \sigma_i^\dagger \sigma_i$ are the photon number and the number of excitations of the atomic levels, respectively. $a_i^\dagger$ and a_i are respectively the photon creation and annihilation operators at lattice site i. The Pauli matrices $\sigma_i^\dagger$ (σ_i) represent the raising (lowering) operator. U is the atom-photon coupling strength. Note that the total particle number $N = N_a + N^\sigma$ is conserved [U(1) symmetry] within this approach. As shown in Fig. 1, $a_i \sigma_i^\dagger$ means that a photon is absorbed and an atom excitation forms simultaneously, and may hence be understood as a raising operator in a pseudo-spin-1/2 space formed by the two states $|g, 1\rangle_x$ and $|e, 0\rangle_x$. For convenience, we focus on the case $\varepsilon = \omega = 0$.

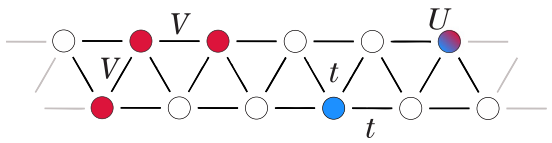

FIG. 2. Sketch of the extended JCH model on a triangular cavity ladder geometry.

In this study, we focus our analysis on a sector of low density of excitations $\rho \leqslant 1$, where at most one photon is present in each cavity. As we will show, this regime can be modeled by a hard-core particle description with at most one photon per cavity.

The extended JCH model includes a dipole interaction term and photon tunneling term between cavities. The Hamiltonian is defined as

$$H = \sum_i \left(H_i^{\mathrm{JC}} - \mu n_i\right) - t \sum_{\langle i,j \rangle} (a_i^\dagger a_j + \mathrm{H.c.}) + \sum_{\langle i,j \rangle} V n_i^\sigma n_j^\sigma, \tag{2}$$

where the total number of excitations is $\rho \equiv \sum_i n_i = \sum_i (n_i^\sigma + n_i^a)$, μ is the chemical potential, t is the hopping amplitude of photons between a pair of neighboring lattice sites i and j, and V is the nearest-neighbor interaction between the atoms. The main ingredients of model (2) are sketched in Fig. 2 for a zigzag-ladder geometry.

In the limit of a dominant atom-photon coupling $U \gg V$ and t when fillings $\rho < 1$, one may project model (2) to its low-energy subspace composed of sites with on-site singlets $(|g, 1\rangle_x - |e, 0\rangle_x)/\sqrt{2}$ and empty sites $|g, 0\rangle_x$, after identification of the states $|1\rangle_x^b$ and $|0\rangle_x^b$ in a (hardcore) BH model. Hence a first-order approximation map model (2) is given by the following Hamiltonian:

$$H_{\mathrm{BH}} = \sum_i (-U - \mu) n_i^b - \frac{t}{2} \sum_{\langle i,j \rangle} (b_i^\dagger b_j + \mathrm{H.c.}) + \frac{V}{4} \sum_{\langle i,j \rangle} n_i^b n_j^b, \tag{3}$$

with bosonic annihilation (creation) operators b_i ($b_i^\dagger$) and $n_i^b = b_i^\dagger b_i$. The properties of model (3) have been studied extensively in various lattice geometries, for example, Refs. [35–39]. In the following, we focus on the properties of the model (2) in the regime $t < V \lesssim U$.

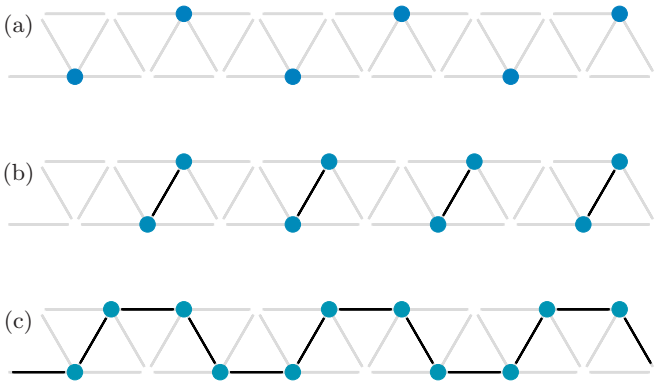

FIG. 3. Sketch of the typical density configurations (blue bullets) for the ladder for the (a) $\mathrm{DW}_{1/3}$ phase ($t/U = 0.01,\ \mu/U = -0.88$), (b) $\mathrm{DW}_{1/2}$ phase ($t/U = 0.01,\ \mu/U = -0.82$), and (c) $\mathrm{DW}_{2/3}$ phase ($t/U = 0.01,\ \mu/U = -0.74$). The black lines indicate the strength of the nearest-neighbor density correlations $\langle n_i^b \rangle \langle n_j^b \rangle$ (one-site MF simulation; see below).

III. EXTENDED JCH MODEL ON TRIANGULAR ZIGZAG LADDERS

In the following, we study the JCH model on quasi-1D zigzag ladders. As sketched in Fig. 2 this model resembles a two-leg ladder stripe of the 2D triangular lattice. It can be also seen as a 1D chain with nearest- and next-nearest-neighbor couplings.

A. Limit of vanishing intercavity hopping $t/U \to 0$

The limit of a vanishing tunneling $t \to 0$ in the ground states of the (extended) BH model such as Eq. (3) are given by classical particle configurations. At a fixed filling, the ground-state manifold is yet typically highly degenerate as excitations are localized at some lattice site. For certain filling fractions, e.g., on zigzag ladder $\rho = 1/3,\ \rho = 1/2$, and $\rho = 2/3$, the degeneracy is lifted, where a DW pattern minimizes the interaction energy V. Therefore, only those filling fractions remain stable in a grand-canonical ensemble. The lattice configurations of the extended JCH model in the $t \to 0$ limit resemble the ones of the extended BH model physics with stable plateaus at fillings $\rho = 1/3,\ \rho = 1/2$, and $\rho = 2/3$, and a macroscopic degeneracy for the remaining fillings. We sketch the configurations in Fig. 3. If we consider the zigzag ladder as a 1D chain with nearest- and next-nearest-neighbor couplings, the DW pattern can be described by the following periodic classical Fock state of excitations $|1\rangle$ and empty sites $|0\rangle$: the $\mathrm{DW}_{1/3}$ phase at $\rho = 1/3$ is given by $|\ldots, 1, 0, 0, \ldots\rangle$, the $\mathrm{DW}_{1/2}$ phase at $\rho = 1/2$ by $|\ldots, 1, 1, 0, 0, \ldots\rangle$, and the $\mathrm{DW}_{2/3}$ phase at $\rho = 2/3$ by $|\ldots, 1, 1, 0, \ldots\rangle$. An important difference between the quasi-1D ladder geometry and the 2D lattices is that, in the triangular two-leg ladder, the solid density wave phase at half-filling can be found in addition to the solid phases at fillings 1/3 and 2/3. The emergence and properties of these solid phases for the BH limit have been studied in various works, e.g., Refs. [38,39].

Due to the interplay between U and V, the JCH model, however, obviously exhibits a nontrivial physics in the pseudospin sector even for strict $t = 0$ limit. The V term leads to Ising-like interactions of excitation on neighboring sites. Expressing the states $|g, 1\rangle_j$ as a spin $|\downarrow\rangle_j$ and $|e, 0\rangle_j$ as $|\uparrow\rangle_j$, we may express the Hamiltonian of the pseudospin degree of freedom as an Ising model with a transverse and longitudinal field

$$H_{1/2} = V \sum_{\langle j,j' \rangle} \left(S_j^z - \frac{1}{2} \right) \left(S_{j'}^z - \frac{1}{2} \right) + U \sum_j S_j^x, \qquad (4)$$

where the sum $\langle j, j' \rangle$ runs over neighboring occupied sites. The $\mathrm{DW}_{1/3}$ and $\mathrm{DW}_{1/2}$ phases form pseudospin singlets of single occupied or neighboring site occupations, while interestingly the $\mathrm{DW}_{2/3}$ phase exactly maps to the 1D Ising model. As model (4) is nonintegrable for $U \neq 0$, we calculate the ground-state energies by means of DMRG [40,41] simulations and obtain the generic phase diagram Fig. 4 of the JC model on the zigzag ladder.

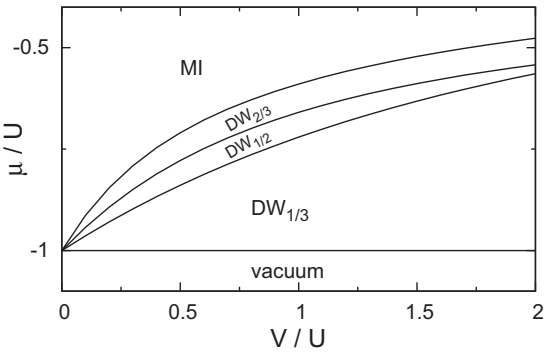

FIG. 4. Phase diagram of the extended JCH model on a quasi-1D zigzag ladder (DMRG simulations) in the limit of vanishing cavity coupling $t = 0$, as discussed in the text, as a function of the chemical potential μ and the nearest-neighbor interaction V.

B. Phase diagram at finite $t/U \geqslant 0$

In the following, we study the JCH model on quasi-1D zigzag ladders at finite $t \geqslant 0$ and intermediate strength interactions $V \lesssim U$. We employ DMRG simulations with open boundary conditions keeping up to $m = 1000$ matrix states in the sector of a fixed number of excitations ρ. We calculate several observables and correlation functions to characterize the various ground-state phases.

In Fig. 5, we present the phase diagram of the extended JCH model on the zigzag ladder anticipating the discussion of the following section in the $\mu - t$ plane for $V = 0.4U$ and for small fillings $\rho < 1$. A finite hopping $t/U > 0$ will generally destabilize the gapped phases and induces a transition of a gapless phase, which is an ordinary single component (superfluid) Luttinger-liquid–like phase of photons tunneling between the cavities (SF). Interestingly, we also find an extended region around the $\mathrm{DW}_{1/2}$ lobe, which we call a pair-supersolid phase (P-SS), which will be discussed below in more detail.

Figure 6 shows the equation of state $\rho = \rho(\mu)$ for several cuts through the phase diagram of Fig. 5. The dashed horizontal lines depict the commensurate fillings $\rho = 1/3,\ 1/2$, and 2/3 for which we observe the gapped density wave phases, characterized by a plateau in the $\mu - \rho$ curve and a vanishing compressibility. Note that, due to finite-size effects and the

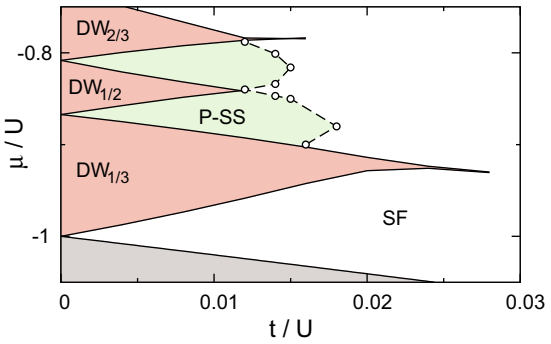

FIG. 5. Phase diagram of the extended JCH model on a quasi-1D zigzag ladder (DMRG simulations, $V/U = 0.4$). We observe several gapped DW phases at fillings 1/3, 1/2, and 2/3, as well as a MI region at unit filling (not shown). The green shaded regions mark the pair-supersolid (P-SS) surrounding the $DW_{1/2}$ phase (see text).

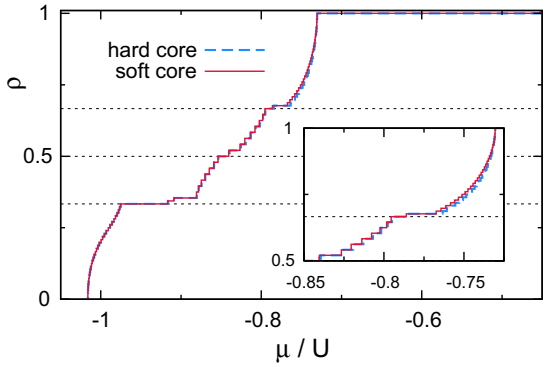

FIG. 7. $\mu - \rho$ curve for the extended JCH model on a quasi-1D zigzag ladder (DMRG simulations, $V/U = 0.4$, $L = 96$ sites, $t/U = 0.008$) for the hard-core and the soft-core JCH model (allowing for the occupation of two photons per cavity). Within the given parameters both curves coincide almost perfectly.

conservation of the total particle number $N = N_a + N^\sigma$, the $\mu - \rho$ curve is not smooth but consists of small steps ΔN and we observe a splitting of the plateaus into two levels at filling of N particles on L sites as well as $N + 1$ or $N + 2$.

While for the previous results we studied the hard-core JCH model, experimentally, of course, the presence of more than one photon per cavity cannot be excluded. However, as can be seen in Fig. 7, this effect plays a minor role in the low density regime studied in this work. Relaxing the hard-core constraint only leads to a minor shift in the $\rho - \mu$ curves of Fig. 7.

C. Pairing

The paired phase can be identified in the $\mu - \rho$ curve of Fig. 6 by the presence of steps of $\Delta N = 2$, compared to the ordinary SF phase with steps $\Delta N = 1$. This feature is typical for phases of paired particles, where the two-particle excitation energy ΔE_2 becomes lower than the ΔE_1 which is due to a gain in binding energy. Here we may define

$$\Delta E_\nu = \frac{E(N-\nu) - 2E(N) + E(N+\nu)}{\nu}, \tag{5}$$

with the ground-state energy $E(N)$ of a system of N excitations on L sites. In Fig. 8 we show the gaps ΔE_1 and ΔE_2 for a cut through the phase diagram of Fig. 5 at fixed density. In the P-SS phase ΔE_1 remains finite in the thermodynamic limit, while ΔE_2 vanishes, showing the gapless paired character of the phase. In order to further characterize the P-SS and SF phases, we calculate correlation functions. In both previous Luttinger-liquid phases, the atom excitation correlation $C_n^\sigma(r)$ and the photon density correlation $C_n^a(r)$ decay with an inverse power law [42–44], where $C_n^\sigma(r)$ and $C_n^a(r)$ are defined by

$$\begin{aligned} C_n^\sigma(r) &= \langle n_i^\sigma n_{i+r}^\sigma \rangle - \langle n_i^\sigma \rangle \langle n_{i+r}^\sigma \rangle, \\ C_n^a(r) &= \langle n_i^a n_{i+r}^a \rangle - \langle n_i^a \rangle \langle n_{i+r}^a \rangle. \end{aligned} \tag{6}$$

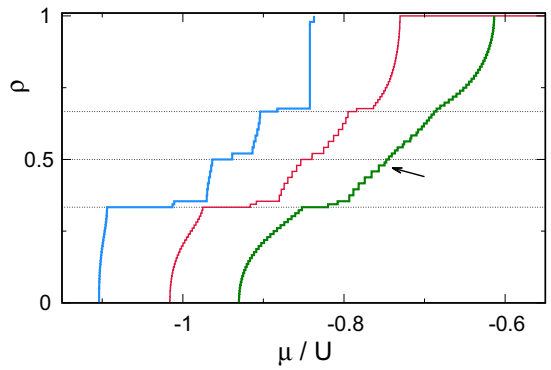

FIG. 6. $\mu - \rho$ curve for the extended JCH model on a quasi-1D zigzag ladder (DMRG simulations, $V/U = 0.4$, $L = 96$ sites) for different values of $t/U = 0.002$, $t/U = 0.008$, and $t/U = 0.015$ (from left to right). The curves have been shifted by 0.1 among each other for clarity. The paired phase can be seen in this diagram by the presence of steps of $\Delta N = 2$. The arrow marks the transition to the SF phase with $\Delta N = 1$ for the $t/U = 0.015$ curve.

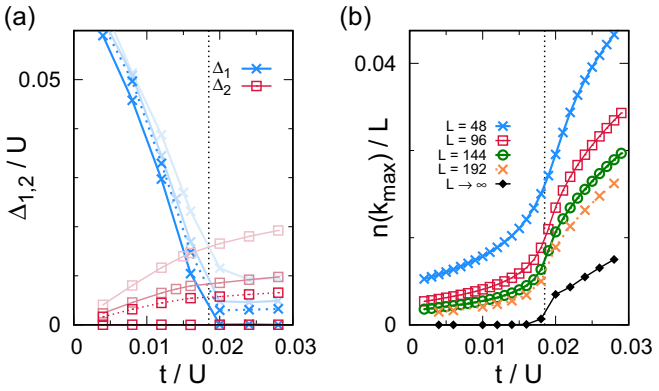

FIG. 8. Cuts through the phase diagram of Fig. 5 for a fixed density $\rho = 5/12$. (a) Single- and two-particle excitation gap ΔE_1 and ΔE_2 for (top to bottom and light to dark colors) $L = 48$, 96, and 144 sites as well as the extrapolation to the thermodynamic limit. (b) (Single-particle) momentum distribution for different system sizes $L = 48$, 96, 144, and 192. The lower black line is the extrapolation to the thermodynamic limit using a higher-order polynomial.

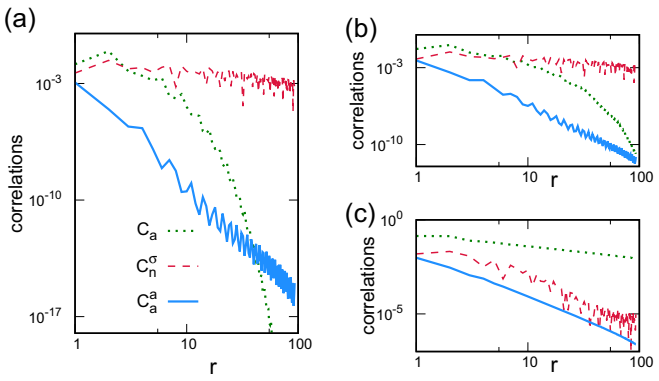

FIG. 9. DMRG method detailed description of the extended JCH model on the triangular zigzag ladder with $V/U = 0.4$, $\rho = 0.416$ ($L = 192$ sites) for (a) $t/U = 0.004$ (P-SS phase), (b) $t/U = 0.012$ (P-SS), and (c) $t/U = 0.026$ (SF). While $C_a^\sigma(r)$, $C_n^\sigma(r)$ show always a clear algebraic decay, the single-particle correlation $C_a(r)$ is only algebraic in the SF phase, while exponentially in the P-SS phases.

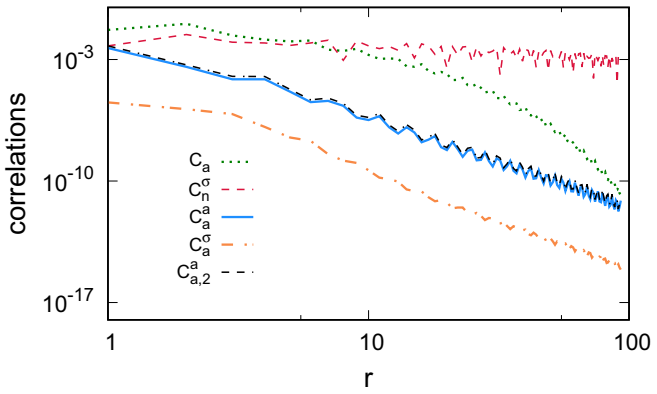

FIG. 10. Various correlation functions in the P-SS phase of the extended JCH model on the triangular zigzag ladder ($V/U = 0.4$, $\rho = 0.416$, $L = 192$ sites, $t/U = 0.012$). DMRG data.

At incommensurate fillings in general, the above correlations emerge in the shape of beats [45,46]. The superfluid order could be denoted by noninteger fillings and power-law decaying of the nondiagonal correlation [42–44]

$$C_a(r) = \langle a_i^\dagger a_{i+r} \rangle. \tag{7}$$

Besides the usual single-particle tunneling correlation, pairing correlations may be defined as

$$\begin{aligned} C_a^\sigma(r) &= \langle a_i^\dagger \sigma_i^\dagger \sigma_{i+r} a_{i+r} \rangle, \\ C_a^a(r) &= \langle a_i^\dagger a_{i+1}^\dagger a_{i+r} a_{i+r+1} \rangle, \\ C_\sigma^\sigma(r) &= \langle \sigma_i^\dagger \sigma_{i+1}^\dagger \sigma_{i+r} \sigma_{i+r+1} \rangle, \\ C_{a,2}^a(r) &= \langle a_i^\dagger a_{i+2}^\dagger a_{i+r} a_{i+r+2} \rangle. \end{aligned} \tag{8}$$

In Fig. 9 we plot the correlations for a fixed density for various tuning rates. While in the SF phases, the density-density correlation C_n, the superfluid single particle C_a, and the pairing correlations $C_a^a(r)$ exhibit an algebraic decay; upon entering the P-SS region, the single-particle correlations C_a decay faster than a power law. The pairing correlations decay fast, but clearly with a power law (corresponding to a line in the log-log plot). For small tunneling rates [Fig. 9(a)] the pairing correlations are also in absolute value exceeding the single-particle correlations. In Fig. 10 we plot the different pairing correlations $C_a^a(r)$, $C_a^\sigma(r)$, $C_{a,2}^a(r)$ for the P-SS phase, which all exhibit the same scaling properties.

Indeed, the presence of the pairing phase for the zigzag ladder may be understood already from the BH limit for a strong atom-photon coupling due to the presence of the solid phase at half filling $\rho = 1/2$ for $t \to 0$. In this limit, we observe that it is energetically favorable in a grand-canonical ensemble to dope the system with an even number of holes such that the total size of domain-wall excitations (in pairs of three lattice sites) becomes commensurate with the original crystalline lattice structure (four lattice sites unit cell). Hence we may understand the dominant pairing correlation observed numerically in the JCH model on a zigzag ladder as reminiscent of this phase. For a minimal handwaving example, one may analogously consider the doping of a single excitation on top of the $DW_{1/3}$, in a schematic picture given by $|\cdots - 00 - 00 - 00 - 00 - 00 \cdots\rangle$, using the nomenclature of Eq. (3). In the limit of $U \gg V$ and $U \gg V$ also, an additional particle creates two domain-wall–like excitations $|\cdots - -0 - 00 - 00 - 00 - 00 \cdots\rangle$ at a cost of $\sim 2V/4 - U - \mu$, which can move through the lattice gaining kinetic energy, e.g., $|\cdots - -00 - 000 - 00 - -00 \cdots\rangle$. Now a second photon can be added, e.g., $|\cdots - -00 - 00 - -00 - -00 \cdots\rangle$, at a lower cost $\sim 3V/8 - U - \mu$. The soft-core character of the JCH model allows one to further lower the energy cost and thus maintain the preservation of the crystalline lattice structure, leading to the formation of a supersolid ordering, as will be shown in the following.

D. Emergence of the supersolid correlations

Interestingly, the P-SS region not only exhibits a strong pairing, but we also find evidence for a supersolidlike ordering. For this, we study the scaling of the structure factor which helps to characterize the solid order [46–52]

$$S(k)^\nu = \sum_{j,j'} \langle n_j^\nu n_{j'}^\nu \rangle \exp[ik(j - j')], \tag{9}$$

where $\nu = \sigma, a$ and both quantities can reflect the solid order. Note that in this paper we define the structure factor (as well as the momentum distribution) for simplicity ordering the lattice sites as a single 1D chain along the zigzag direction. This corresponds to an interpretation of the zigzag ladder as a 1D $J_1 - J_2$ model well described in the literature (compare, e.g., Ref. [38] and references therein). Apart from the trivial peak at $k = 0$, $S(k)$ has a second pronounced peak at $k_{\max} = \pm 2/3\pi$ for the gapped DW phase. Also in the gapless P-SS phase, we observe a pronounced second maximum $S(k_{\max})$ which is shifted slightly away from $k_{\max} = \pm 2/3\pi$. Examples for the structure factor are shown in Fig. 11(a). This peak indicates the presence of a density ordering in the liquid phase, which defines a supersolid. In Fig. 11, we also plot the Fourier transform of the $C_a(r)$, namely, the momentum distribution

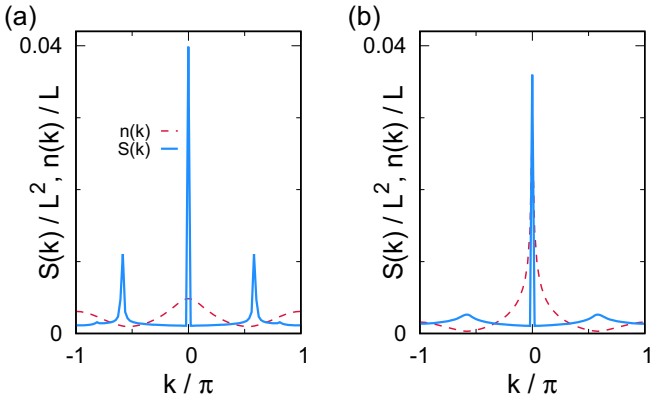

FIG. 11. Structure factor $S(k)$ and momentum distribution $n(k)$ for the zigzag ladder for $\rho = 5/12$, $V/U = 0.4$ and (a) $t/U = 0.008$, P-SS phase, and (b) $t/U = 0.026$, SF phase ($L = 96$ sites, DMRG simulation). For (a), in the P-SS the third local maximum of the structure factor is also observed.

is defined as

$$n(k) = \frac{1}{L}\sum_{j,j'}\langle a_j^\dagger a_{j'}\rangle \exp[ik(j-j')], \tag{10}$$

which was observed experimentally [5]. The exponential suppression of the single-particle correlations may also be seen by the blurring of the momentum distribution in the P-SS phase.

Following Refs. [47–50], we study the scaling of the peak height of the structure factor $S(k_{\max})$ with the system size. As shown in Fig. 12(a), an extrapolation to the thermodynamic limit of the maximum structure factor $S(k_{\max})$ is performed with different sizes for a cut through the phase diagram of Fig. 5. The structure factor $S(k_{\max})$ remains finite in the P-SS phase and vanishes after the transition to the SF region.

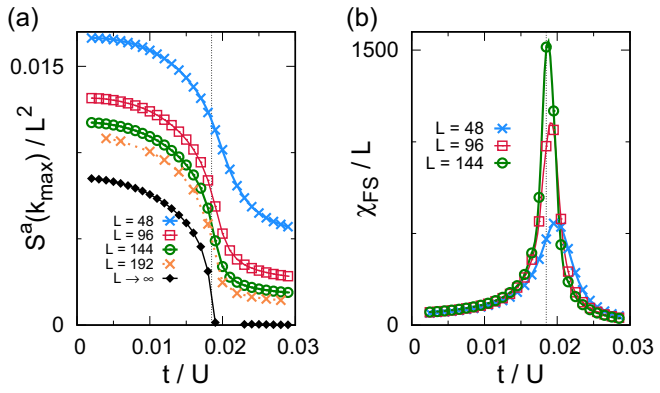

FIG. 12. Cuts through the phase diagram of Fig. 5 for a fixed density $\rho = 5/12$. (a) DW order in the SS phase. Scaling of the peak maximum of the structure factor in Eq. (9) $S(k_{\max})$ for different system sizes $L = 48$, 96, 144, and 192. The lower black line is the extrapolation to the thermodynamic limit using a higher-order polynomial. (b) Scaling of the fidelity susceptibility $\chi_{\rm FS}/L$ according to Eq. (11) across the P-SS to SF phase transition.

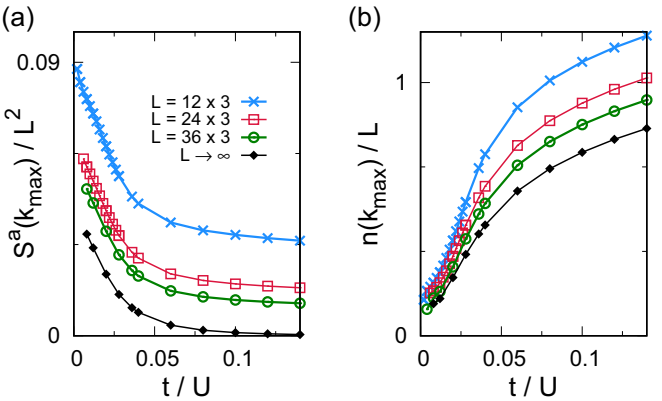

FIG. 13. Scaling of the peak maximum of the structure factor in Eq. (9) $S(k_{\max})$ for different system sizes $L = 12 \times 3$, 24×3, and 36×3 sites of the three-leg ladder JCH model for a fixed density $\rho = 5/12$ ($U = 1$, $V = 0.4$). The lower black line is the extrapolation to the thermodynamic limit using a higher-order polynomial.

The phase transition point may be further classified by a study of the fidelity susceptibility [53]

$$\chi_{\rm FS}(t) = \lim_{\delta t\to 0}\frac{-2\,\ln|\langle\Psi_0(t)|\Psi_0(t+\delta t)\rangle|}{(\delta t)^2}, \tag{11}$$

with the ground-state wave function $|\Psi_0(t)\rangle$, a tunneling parameter t, and a small parameter δt. In Fig. 12(a) we observe the emergence of distinct divergent peaks of $\chi_{\rm FS}/L$ close to the phase transition between the P-SS and SF phase. The roughly linear scaling of $\chi_{\rm FS}/L$ with the system size hints at an Ising character of the phase transition between the two regimes.

IV. THREE-LEG TRIANGULAR LADDER

As argued above, the pairing and the emergence of the P-SS phase is an intrinsic property of the two-leg ladder limit and, hence, we do not expect the pairing still to be present in the three three-leg ladder or 2D case. It is, hence, an interesting question what happens to the supersolidity in the absence of pairing. Therefore, before proceeding to the 2D lattice we extend our DMRG results and study the presence of a supersolid phase in the three-leg ladder limit. We study the three-leg ladder JCH model for again the low-density hardcore limit at a fixed low density $\rho = 5/12$ intermediate between $\rho = 1/3$ and $\rho = 1/2$ filling. The results are shown in Fig. 13.

We observe a distinct peak in the structure factor at $k = 2\pi/3$ (not shown) which extrapolates to a finite value in the thermodynamic limit as shown in Fig. 13. We do not find the signatures of a pairing phase. As expected, the single-particle momentum distribution remains finite for the region with a density order, indicating the presence of a supersolid phase. Due to the absence of pairing, the transition between the SS and the SF phase is apparently very different for the three-leg ladder case. The transition to the SF phase is very smooth contrary to the two-leg ladder model, where a sharp (potentially Ising-like) transition was observed. Interestingly, the supersolid order remains finite for much larger values of the hopping amplitude $t \sim 0.1U$. This may indicate the interesting possibility of a stable light-supersolid phase also

in the 2D limit, as we will examine in the following. Further details of the three-leg ladder model will be studied elsewhere.

V. CMF RESULTS FOR TRIANGULAR LATTICES

A. Cluster mean-field method

The single-site MF has successfully predicted the SF-MI phase transition without long-range interaction ($V = 0$) [54]. The cluster mean-field (CMF) will be more reliable in predicting the physics in the interaction systems ($V \neq 0$) [55–58]. The basic idea is to divide the system into N_c unit cells, periodically patterning an infinite lattice, and each unit cell contains nc sites. The Hamiltonians within each cell are treated exactly and the Hamiltonians between each cell are approximated by $AB \approx A\langle B\rangle + \langle A\rangle B - \langle A\rangle\langle B\rangle$.

The total Hamiltonian can be considered as a sum over the local Hamiltonians on each unit cell, which contain the parts H^c_{in}, which are treated exactly, and the CMF Hamiltonian $H^c_{\rm MF}$ as follows:

$$H = \sum_{c=1}^{N_c} \left(H^c_{\rm in} + H^c_{\rm MF}\right). \tag{12}$$

The Hamiltonian $H^c_{\rm in}$ can be expressed as

$$H^c_{\rm in} = -zt \sum_{i,j\in c} (a_i^\dagger a_j + {\rm H.c.}) + zV \sum_{i,j\in c} n_i^\sigma n_j^\sigma + \sum_{i\in c} h_i, \tag{13}$$

where $h_i = -\mu_p n_i^a - (\Delta + \mu_s) n_i^\sigma + U(\sigma_i^\dagger a_i + a_i^\dagger \sigma_i)$ and the sum runs over all n_c cluster sites. The chemical potential of photons is μ_p and the chemical potential of atoms is μ_s, and the different labels of chemical potential are convenient to test our codes. In actual simulations, $\mu_p = \mu_s = \mu - \omega$, $\Delta = \omega - \varepsilon$, and Δ are maintained at zero for convenience.

The Hamiltonian $H^c_{\rm MF}$ is given by

$$H^c_{\rm MF} = -qt \sum_{i,j\in ce} [(a_i^\dagger + a_i)\Psi_j + (a_j^\dagger + a_j)\Psi_i - 2\Psi_i\Psi_j] + qV \sum_{i,j\in ce} \left(n_i^\sigma \rho_j^\sigma + n_j^\sigma \rho_i^\sigma - \rho_i^\sigma \rho_j^\sigma\right), \tag{14}$$

where z is equal to 1, the chosen setting in Ref. [34], $q = 2z$ for the triangular lattices, $\Psi_i = \langle a_i\rangle$ is the superfluid order parameter, and $\rho_i^\sigma = \langle n_i^\sigma\rangle$ is the number of atomic excitations. Here the sum over ce runs over the bonds between the different clusters.

By systematically scaling the cluster size nc, one may obtain quantitative exact results for 2D systems when comparing to more extensive QMC studies [26,27,59]. Therefore, we consider different cluster sizes and tessellations of the triangular lattice to examine the stability of our findings. In Fig. 14, we exemplify different cluster sizes employed in the study.

In practice, we determine the self-consistent solutions ρ_i^σ and Ψ_i by iterative calculation of the ground state of the cluster system until the mean fields have converged. While for small cluster sizes such as Fig. 14(e) the ground state of the cluster may be obtained by exact-diagonalization techniques, for the larger cluster sizes we employ the DMRG simulation. Following Ref. [60] in this MF scheme already a low number of matrix states is sufficient. In the present examples we choose 30 and 60 states for $nc = 12$ site cluster results shown below.

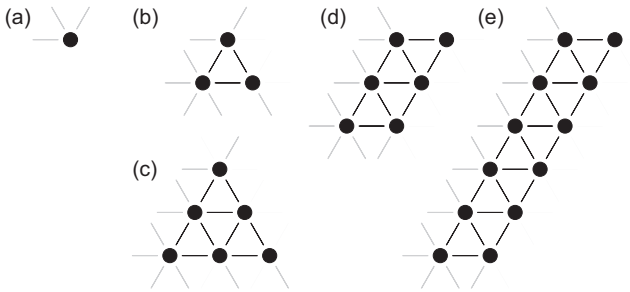

FIG. 14. Examples of different cluster geometries employed in the simulations: single site MF cluster (a) with $nc = 1$ and $N_c = 36$ one-site MF sites, triangular clusters [(b) with $nc = 3$ and (c) with $nc = 6$] with $N_c = 2$, and square tessellations [(d) with $nc = 6$ and (e) with $nc = 12$ sites] with $N_c = 3$ independent clusters.

The solid or density wave orders denoted by $\delta\rho^a$, $\delta\rho^\sigma$, and $\delta\Psi$ are defined by the averaged local order parameters:

$$\delta A = \frac{1}{Nc\cdot nc} \sum_{c,i\in c} |\langle A_i\rangle - \bar{A}|, \quad \bar{A} = \frac{1}{Nc\cdot nc} \sum_{c,i\in c} \langle A_i\rangle. \tag{15}$$

So, e.g., $\delta\Psi = \frac{1}{Nc\cdot nc}\sum_{c,i\in c} |\langle a_i\rangle - \bar{a}|$. The sum runs over all nc sites in all Nc clusters c. We also define the total excitation $\rho = \rho^a + \rho^\sigma$ [16] and $\delta\rho = \frac{1}{2}(\delta\rho^a + \delta\rho^\sigma)$.

B. MF results for the triangular lattice

In analogy to the zigzag ladder case, by increasing μ, the density ρ will undergo platforms with values of $1/3$, $2/3$ with solid patterns shown in Fig. 15. A solid phase at half filling is not present in the 2D case. In a grand-canonical ensemble, the two solid phases exhibit a direct transition at $t \to 0$ with all states where $1/3 < \rho < 2/3$ is macroscopically degenerate in this classical limit.

In Fig. 16 and Fig. 17 we present the results of one-site MF (or Gutzwiller MF, $nc = 1$) simulations. In order to reproduce different crystalline phases we use a large number of independent sites $N_c = 6 \times 6$ (results for $N_c = 3 \times 3$, not shown, are the same). We observe the two solid phases $\mathrm{DW}_{1/3}$

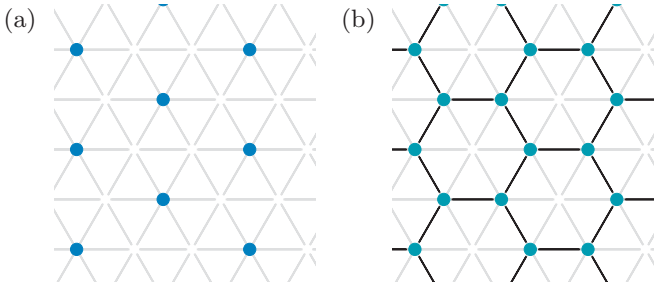

FIG. 15. Sketch of the typical density configurations (blue bullets) for (from one-site method) the (a) $\mathrm{DW}_{1/3}$ phase ($t/U = 0.015$, $\mu/U = -0.9$) and (b) $\mathrm{DW}_{2/3}$ phase ($t/U = 0.015$, $\mu/U = -0.7$). The black lines indicate the strength of the nearest-neighbor density correlations $\langle n_i^b\rangle\langle n_j^b\rangle$.

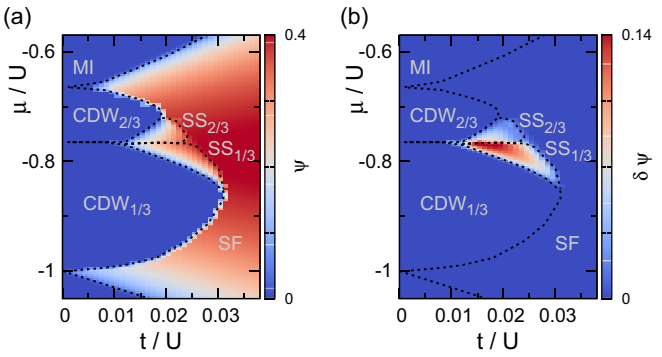

FIG. 16. Schematic phase diagram of the JCH model as obtained from the one-site MF approach ($N_c = 6 \times 6$) in the $\mu - t$ plane for $V/U = 0.4$. The colors depict the (a) superfluid order parameter Ψ and (b) supersolid order $\delta\Psi$.

and $DW_{2/3}$ for a finite atom-photon coupling U in the limit of small $t \ll U$. The typical density patterns are shown in Fig. 17. As shown in Fig. 16, due to the coupling between atoms and photons, the $DW_{1/3}$ and $DW_{2/3}$ phases are not symmetric with $\mu/U = -0.77$, which is an important difference to the particle hole symmetry of the hardcore bosons on the triangular lattices [35–37].

Interestingly, as shown in Fig. 16, two SS phases appear between the $DW_{1/3}$ and $DW_{2/3}$ phases with $\delta\Psi \neq 0$. Sketches of the two different SS patterns are shown in Fig. 17. The hardcore BH model on the triangular lattices has been studied in Refs. [35–37] on triangular lattices for a finite hopping $|t| > 0$ and the emergence of supersolid phases stabilized by an order-by-disorder mechanism for intermediate fillings $1/3 < \rho < 2/3$ has been shown. Also here, the SS phase could be understood in terms of photon tunneling breaking the degeneracy between the $DW_{1/3}$ and $DW_{2/3}$ phases. Hence the emergence of such a SS phase may be based on an order-by-disorder mechanism as conjectured for the BH limit [35–37].

C. Stability of the mean-field results with the cluster size

To illustrate the above results with more detail and study the stability of the one-site MF results, we increase the size of the clusters nc and scan the phase diagram along the lines with different values of t/U. As an example, we choose

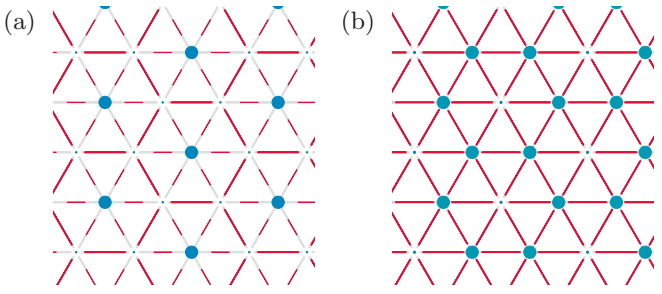

FIG. 17. Sketch of the typical density configurations (blue bullets) for (from one-site MF method) the (a) $SS_{1/3}$ phase ($t/U = 0.022$, $\mu/U = -0.79$) and (b) $SS_{2/3}$ phase ($t/U = 0.022$, $\mu/U = -0.74$). The red lines indicate the strength of the bond kinetic energy $|\langle a_i^\dagger \rangle \langle a_j \rangle|$.

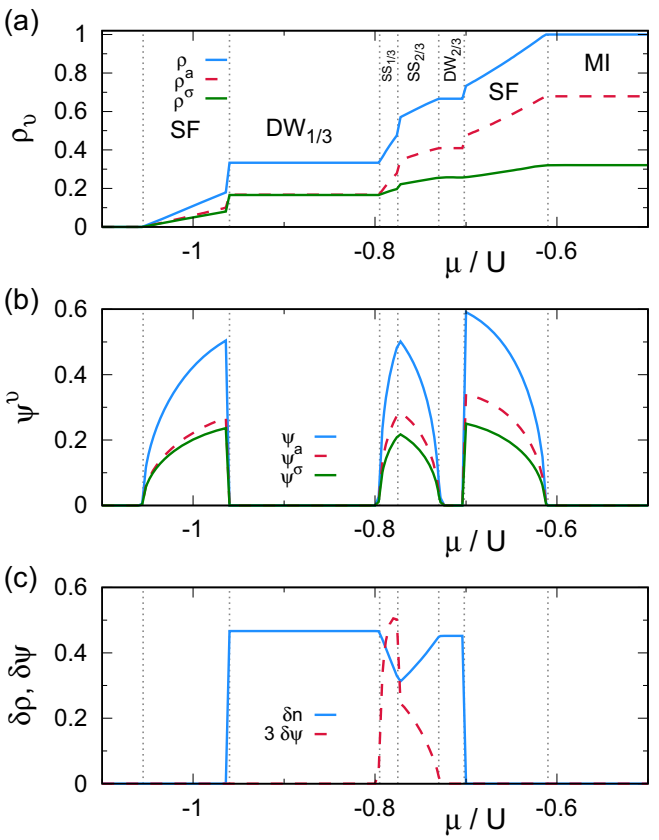

FIG. 18. CMF method detailed description of the (a) total density ρ, and density of photons and excitations ρ^a and ρ^σ, (b) SF order Ψ, Ψ^a and Ψ^σ, and (c) (super)solid order $\delta\rho$ and $\delta\Psi$ vs μ/U with $V/U = 0.4$, $t/U = 0.018$ on the triangular lattices. CMF data for clusters of three-site triangular shape (B in Fig. 14).

$t/U = 0.018$ in Fig. 18 obtained now by a three-site CMF simulation. Starting at $\mu/U \approx -0.95$ and increasing μ/U to -0.8, the system is in the DW phase with $\rho = 1/3$, $\Psi = 0$, and $\delta\rho = 0.44$. With a further increase of μ/U, the three quantities Ψ, $\delta\Psi$, and $\delta\rho$ become nonzero continuously, and the system enters into a SS phase. Since this SS phase is understood from particle doping on the $DW_{1/3}$ phase, we therefore denote it as a $SS_{1/3}$ phase.

By increasing μ/U to -0.75, the quantities ρ and $\Delta\Psi$ jump to nonzero values and the system enters into another SS phase. This SS phase could be called $SS_{2/3}$, because it is formed by hole doping on the solid $DW_{2/3}$. The phase transition of $SS_{1/3}$ to $SS_{2/3}$ is first order. This is consistent with previous work [61,62], in which the two SS phases of hardcore bosons take place according to first-order transitions. By continued increase of μ/U to -0.7, it is obvious that Ψ becomes nonzero, which means that the first-order $DW_{2/3}$-SF phase transition takes place.

In previous works, the nearest [44] or next to nearest [63] repulsive interactions are the necessary conditions for the formation of the supersolid. It should be noted that in our model, even though there is no interaction between photons, the light supersolid emerges, because the repulsion of atoms will cause the effect of repulsion between photons due to atom-photon coupling. This affected atom photon can be

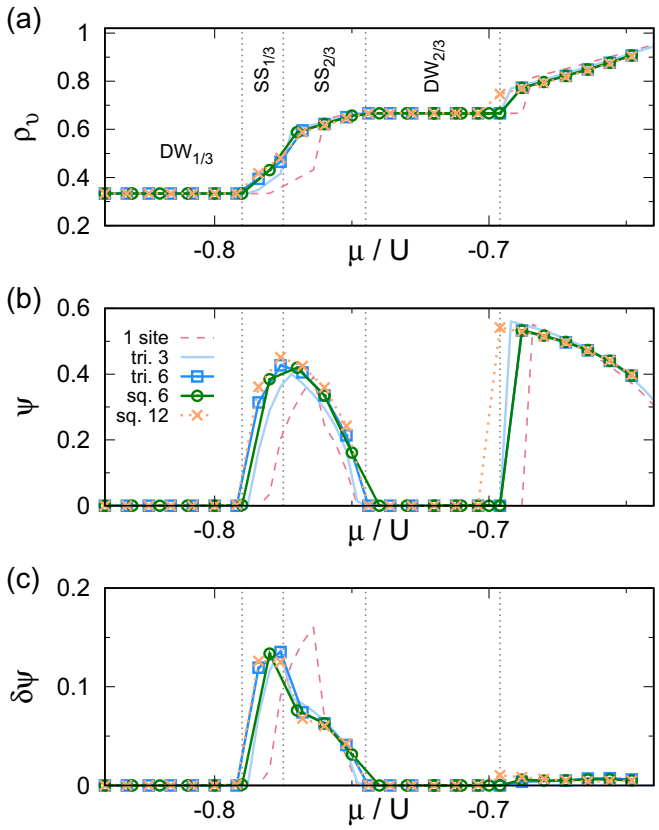

FIG. 19. Comparison and scaling of the CMF results for various cluster sizes for (a) the density ρ, (b) the SF order Ψ, and (c) the supersolid order $\delta\Psi$ vs μ/U with $V/U = 0.4$, $t/U = 0.015$ on the triangular lattice. The different curves show the one-site MF simulation (simulation of a $N_c = 36$ site-unit cell), different clusters of triangular shape (B and C in Fig. 14 with $nc = 3$ and $nc = 6$ sites, $N_c = 2$), and square parketting (D and E in Fig. 14 with $nc = 6$ and $nc = 12$ sites, $N_c = 3$).

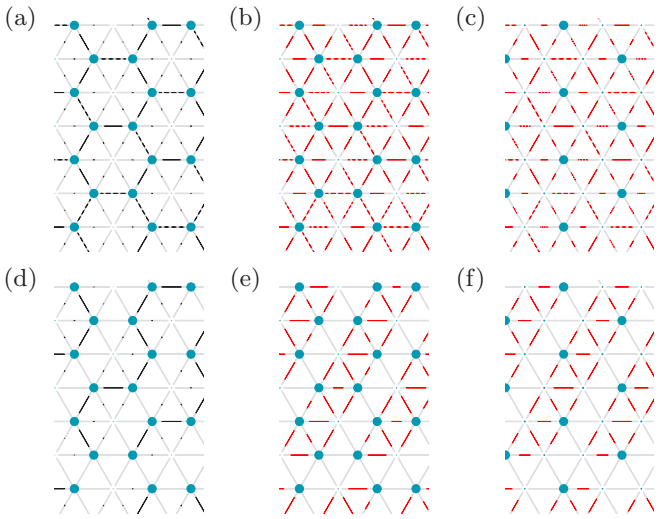

FIG. 20. Sketch of the typical density configurations (blue bullets) for (from the 12-site MF method) the (a) and (d) $DW_{2/3}$ phase ($t/U = 0.015$, $\mu/U = -0.72$), (b) and (e) $SS_{2/3}$ phase ($t/U = 0.015$, $\mu/U = -0.752$), and (c) and (f) $SS_{1/3}$ phase ($t/U = 0.015$, $\mu/U = -0.784$). The black lines indicate the strength of the nearest-neighbor density correlations and bond kinetic energy: (a)–(c) the disconnected part $\langle n_i^b\rangle\langle n_j^b\rangle$ and $|\langle a_i^\dagger\rangle\langle a_j\rangle|$ and (d)–(f) the connected two-site correlators in the clusters $\langle n_i^b n_j^b\rangle$ and $|\langle a_i^\dagger a_j\rangle|$.

verified by calculation of the expectation values of $\sigma_i^\dagger a_i$ or $\sigma_i a_i^\dagger$, which is nonzero even when the system is in the $DW_{1/3}$, $DW_{2/3}$, and MI($\rho = 1$) phases, where $\Psi = 0$ (not shown). The behaviors of $\langle\sigma_i^\dagger a_i\rangle \neq 0$ and $\langle\sigma_i^\dagger\sigma_{i+1}^\dagger\rangle \neq 0$ mean that a type of fluctuation with transitions between atom excitations and photons remains in the system.

Within the given range of parameters and observables our results remain stable with increasing the cluster size. As exemplified in Fig. 19 already the one-site MF approach may qualitatively reproduce the main features of the phase diagram, compared to the CMF results. The three-site and six-site CMF results already give quantitatively good agreement and the 12-site data mainly overlaps with the six-site results. Interestingly, we observe only a small difference between the two different tessellations with six-site clusters of Figs. 14(c) and 14(d) employed in the CMF simulation. In particular, the size of the SS phases increases slightly with the cluster size, which indicates that this phase may be stable in the 2D triangular JCH model.

In Fig. 20 we finally show the local patterns of density and superfluid ordering for the $DW_{2/3}$, the $SS_{2/3}$, and the $SS_{1/3}$ phases obtained by the 12-site CMF method. Both local and two-site correlations show similar patterns and compare already well to the one-site MF data shown in Figs. 15 and 17.

We want to note that our CMF findings should be complemented by a QMC study of the model to analyze the stability and properties of the supersolid phases in more detail. However, this goes beyond the scope of this work and will be discussed elsewhere.

VI. DISCUSSION AND CONCLUSIONS

We perform a systematic study of the extended JCH model on triangular lattices and find that the light supersolid is stable in coupled cavities in the thermodynamic limit even when the photon hopping term is considered.

Specifically, the JCH model on the two-leg triangular ladders is studied by the powerful DMRG method. We find a pairing caused by the interplay between the atoms in the cavities and the atom-photon interaction in the two-leg triangular ladders. The quantities such as single (two) -particle binding energy $\Delta E_{1(2)}$, single-particle correlation $C_a(r)$, and various pairing correlations $C_a^\sigma(r)$, $C_a^a(r)$, $C_\sigma^\sigma(r)$, and $C_{a,2}^a(r)$ are shown. To see clearly the behaviors of these correlations, we calculate the systems with sizes up to $L = 192$. We also find that, for small tunneling rates, the pairing correlations are also in absolute value exceeding the single-particle correlations. The existence of the pair supersolid is also verified by the finite-size scaling of structure factor and momentum distribution, in combination of previous pair correlations. The P-SS to SF phase transition has Ising character by the study of the fidelity susceptibility $\chi_{FS}(t)/L$.

To clarify the question of whether or not the P-SS phase exists in the JCH model on the triangular ladders with more

legs, we implement the DMRG method to simulate the JCH model on the three-leg triangular ladders. The pairing disappears but the regular supersolid, i.e., solid and single-particle tunneling superfluid, still exists simultaneously. Interestingly the SS phase may be observed for even larger values of t/U. The phase transitions between SS to SF are different from those in the two-leg JCH model, which will be further studied in the future.

The JCH model on the two-dimensional triangular lattices are studied by the cluster mean-field method. The global phase diagram, which contains $DW_{1/3}$, $DW_{2/3}$, $SS_{1/3}$, and $SS_{2/3}$, are presented. The mechanism of the solid could be understood as intercavity tunneling of the photons breaking the degeneracy between solids. For the formation of the SS phase of the BH model, the key is the interaction, which is absent between photons. However, the solid and SS of photons still can form through the atom-photon coupling, which induces an effective interaction between the photons. Different cluster sizes and tessellations of the triangular lattice are used to examine the stability of a supersolid phase. With the increase of cluster size, the parameter ranges of the SS phase are convergent.

To summarize, we have conclusively obtained the P-SS phase of the JCH model on the two-leg triangular ladder and also the SS phase on three-leg triangular ladders and regular triangular lattices. Since the model is free of sign problems, a study of the model by means of the worm quantum Monte Carlo simulations will be published elsewhere. Our results, obtained by the MF and DMRG methods, will be helpful in guiding experimentalists in realizing different and novel quantum phases on optical lattices.

ACKNOWLEDGMENTS

We would like to thank T. C. Scott of BlockFint, Bangkok, Thailand for helping prepare this document. S.G. acknowledges support of Project No. SA 1031/10-1 of the German Research Foundation (DFG) and the Swiss National Science Foundation under Division II. W.Z. is supported by the NSFC under Grant No. 11305113.

[1] O. Penrose and L. Onsager, Bose-Einstein condensation and liquid helium, Phys. Rev. **104**, 576 (1956).
[2] G. V. Chester, Speculations on Bose-Einstein condensation and quantum crystals, Phys. Rev. A **2**, 256 (1970).
[3] A. J. Leggett, Can a Solid Be "Superfluid"? Phys. Rev. Lett. **25**, 1543 (1970).
[4] M. H. W. Chan, R. B. Hallock, and L. Reatto, Overview on solid ^{4}He and the issue of supersolidity, J. Low Temp. Phys. **172**, 317 (2013).
[5] M. Greiner, O. Mandel, T. Dsslinger, T. W. Hänsch, and I. Bloch, Quantum phase transition from a superfluid to a Mott insulator in a gas of ultracold atoms, Nature (London) **415**, 39 (2002).
[6] M. Greiner and S. Föllin, Optical lattices, Nature (London) **453**, 736 (2008).
[7] M. Boninsegni, Phase Separation in Mixtures of Hard Core Bosons, Phys. Rev. Lett. **87**, 087201 (2001).
[8] A. B. Kuklov and B. V. Svistunov, Counterflow Superfluidity of Two-Species Ultracold Atoms in a Commensurate Optical Lattice, Phys. Rev. Lett. **90**, 100401 (2003).
[9] C. Trefzger, C. Menotti, and M. Lewenstein, Pair-Supersolid Phase in a Bilayer System of Dipolar Lattice Bosons, Phys. Rev. Lett. **103**, 035304 (2009).
[10] J. P. Lv, Q. H. Chen, and Y. J. Deng, Two-species hard-core bosons on the triangular lattice: A quantum Monte Carlo study, Phys. Rev. A **89**, 013628 (2014).
[11] J. Léonard, A. Morales, P. Zupancic, T. Donner, and T. Esslinger, Monitoring and manipulating Higgs and Goldstone modes in a supersolid quantum gas, Science **358**, 1415 (2017).
[12] J. Léonard, A. Morales, P. Zupancic, T. Esslinger, and T. Donner, Supersolid formation in a quantum gas breaking a continuous translational symmetry, Nature (London) **543**, 87 (2017).
[13] L. Tanzi, E. Lucioni, F. Fama, J. Catani, A. Fioretti, C. Gabbanini, and G. Modugno, Observation of a Dipolar Quantum Gas with Metastable Supersolid Properties, Phys. Rev. Lett. **122**, 130405 (2019).
[14] F. Böttcher, J. N. Schmidt, M. Wenzel, J. Hertkorn, M. Guo, T. Langen, and T. Pfau, Transient Supersolid Properties in an Array of Dipolar Quantum Droplets, Phys. Rev. X **9**, 011051 (2019).
[15] F. Deppe, M. Mariantoni, E. P. Menzel, A. Marx, S. Saito, K. Kakuyanagi, H. Tanaka, T. Meno, K. Semba, H. Takayanagi, E. Solano, and R. Gross, Two-photon probe of the Jaynes-Cummings model and symmetry breaking in circuit QED, Nat. Phys. **4**, 686 (2008).
[16] J. Koch and K. L. Hur, Superfluid-Mott-insulator transition of light in the Jaynes-Cummings lattice, Phys. Rev. A **80**, 023811 (2009).
[17] D. Underwood, W. Shanks, J. Koch, and A. Houck, Low-disorder microwave cavity lattices for quantum simulation with photons, Phys. Rev. A **86**, 023837 (2012).
[18] K. Toyoda, Y. Matsuno, A. Noguchi, S. Haze, and S. Urabe, Experimental Realization of a Quantum Phase Transition of Polaritonic Excitations, Phys. Rev. Lett. **111**, 160501 (2013).
[19] S. Schmidt, G. Blatter, and J. Keeling, From the Jaynes-Cummings-Hubbard to the Dicke model, J. Phys. B **46**, 224020 (2013).
[20] G. Kulaitis, F. Krüger, F. Nissen, and J. Keeling, Disordered driven coupled cavity arrays: Nonequilibrium stochastic mean-field theory, Phys. Rev. A **87**, 013840 (2013).
[21] C. Nietner and A. Pelster, Ginzburg-Landau theory for the Jaynes-Cummings-Hubbard model, Phys. Rev. A **85**, 043831 (2012).
[22] S. Schmidt and G. Blatter, Strong Coupling Theory for the Jaynes-Cummings-Hubbard Model, Phys. Rev. Lett. **103**, 086403 (2009).
[23] J. Zhang and Y. Jiang, Quantum phase diagrams of the Jaynes-Cummings Hubbard models in nonrectangular lattices, Laser Phys. **27**, 035203 (2017).
[24] A. Mering and M. Fleischhauer, Analytic approximations to the phase diagram of the Jaynes-Cummings-Hubbard model, Phys. Rev. A **80**, 053821 (2009).

[25] A. Souza, B. Sanders, and D. Feder, Fermionized photons in the ground state of one-dimensional coupled cavities, Phys. Rev. A **88**, 063801 (2013).

[26] M. Hohenadler, M. Aichhorn, S. Schmidt, and L. Pollet, Dynamical critical exponent of the Jaynes-Cummings-Hubbard model, Phys. Rev. A **84**, 041608(R) (2011).

[27] J. Z. Zhao, A. W. Sandvik, and K. Ueda, Insulator to superfluid transition in coupled photonic cavities in two dimensions, arXiv:0806.3603.

[28] A. L. C. Hayward, A. M. Martin, and A. D. Greentree, Fractional Quantum Hall Physics in Jaynes-Cummings-Hubbard Lattices, Phys. Rev. Lett. **108**, 223602 (2012).

[29] G. Almeida and A. Souza, Quantum transport with coupled cavities on an Apollonian network, Phys. Rev. A **87**, 033804 (2013).

[30] Y. L. Dong, S. Q. Zhu, and W. L. You, Quantum-state transmission in a cavity array via two-photon exchange, Phys. Rev. A **85**, 023833 (2012).

[31] J. Quach, Disorder-correlation-frequency-controlled diffusion in the Jaynes-Cummings-Hubbard model, Phys. Rev. A **88**, 053843 (2013).

[32] S. Prasad and A. Martin, Effective three-body interactions in Jaynes-Cummings-Hubbard systems, Sci. Rep. **8**, 16253 (2018).

[33] X. F. Zhang, Q. Sun, Y. C. Wen, W. M. Liu, S. Eggert, and A. C. Ji, Superradiant Solid in Cavity QED Coupled to a Lattice of Rydberg Gas, Phys. Rev. Lett. **110**, 090402 (2013).

[34] B. Bujnowski, J. Corso, A. Hayward, J. Cole, and A. Martin, Supersolid phases of light in extended Jaynes-Cummings-Hubbard systems, Phys. Rev. A **90**, 043801 (2014).

[35] S. Wessel and M. Troyer, Supersolid Hardcore Bosons on the Triangular Lattice, Phys. Rev. Lett. **95**, 127205 (2005).

[36] M. Boninsegni and N. Prokof'ev, Supersolid Phase of Hardcore Bosons on Triangular Lattice, Phys. Rev. Lett. **95**, 237204 (2005).

[37] W. Z. Zhang, R. X. Yin, and Y. C. Wang, Pair supersolid of the extended Bose-Hubbard model with atom-pair hopping on the triangular lattice, Phys. Rev. B **88**, 174515 (2013).

[38] T. Mishra, R. V. Pai, and S. Mukerjee, Supersolid in a one-dimensional model of hard-core bosons, Phys. Rev. A **89**, 013615 (2014).

[39] T. Mishra, S. Greschner, and L. Santos, Polar molecules in frustrated triangular ladders, Phys. Rev. A **91**, 043614 (2015).

[40] S. R. White, Density Matrix Formulation for Quantum Renormalization Groups, Phys. Rev. Lett. **69**, 2863 (1992).

[41] U. Schollwoeck, The density-matrix renormalization group, Rev. Mod. Phys. **77**, 259 (2005).

[42] F. D. M. Haldane, Effective Harmonic-Fluid Approach to Low-Energy Properties of One-Dimensional Quantum Fluids, Phys. Rev. Lett. **47**, 1840 (1981).

[43] T. Giamarchi, Resistivity of a one-dimensional interacting quantum fluid, Phys. Rev. B **46**, 342 (1992).

[44] T. D. Kühner, S. R. White, and H. Monien, One-dimensional Bose-Hubbard model with nearest-neighbor interaction, Phys. Rev. B **61**, 12474 (2000).

[45] W. Zhang, S. Greschner, E. Fan, T. C. Scott, and Y. Zhang, Ground state properties of the one-dimensional unconstrained pseudo-anyon Hubbard model, Phys. Rev. A **95**, 053614 (2017).

[46] T. Mishra, R. V. Pai, and S. Ramanan, Supersolid and solitonic phases in the one-dimensional extended Bose-Hubbard model, Phys. Rev. A **80**, 043614 (2009).

[47] G. G. Batrouni, V. G. Rousseau, R. T. Scalettar, and B. Grmaud, Competing phases, phase separation, and coexistence in the extended one-dimensional bosonic Hubbard model, Phys. Rev. B **90**, 205123 (2014).

[48] G. G. Batrouni, R. T. Scalettar, V. G. Rousseau, and B. Grmaud, Competing Supersolid and Haldane Insulator Phases in the Extended One-Dimensional Bosonic Hubbard Model, Phys. Rev. Lett. **110**, 265303 (2013).

[49] J. M. Fellows and S. T. Carr, Superfluid, solid, and supersolid phases of dipolar bosons in a quasi-one-dimensional optical lattice, Phys. Rev. A **84**, 051602(R) (2011).

[50] G. G. Batrouni, F. Hébert, and R. T. Scalettar, Supersolid Phases in the One-Dimensional Extended Soft-Core Bosonic Hubbard Model, Phys. Rev. Lett. **97**, 087209 (2006).

[51] M. Tapan, G. Sebastian, and S. Luis, Frustration-induced supersolids in the absence of intersite interactions, Phys. Rev. B **92**, 195149 (2015).

[52] G. Sebastian and T. Vekua, Vortex-Hole Duality: A Unified Picture of Weak- and Strong-Coupling Regimes of Bosonic Ladders with Flux, Phys. Rev. Lett. **119**, 073401 (2017).

[53] S. Gu, Fidelity approach to quantum phase transitions, Int. J. Mod. Phys. B **24**, 4371 (2010).

[54] D. van Oosten, P. van der Straten, and H. T. C. Stoof, Quantum phases in an optical lattice, Phys. Rev. A **63**, 053601 (2001).

[55] Y. Z. Ren, N. H. Tong, and X. C. Xie, Cluster mean-field theory study of J(1)-J(2) Heisenberg model on a square lattice, J. Phys.: Condens. Matter **26**, 115601 (2014).

[56] D. Yamamoto, Correlated cluster mean-field theory for spin systems, Phys. Rev. B **79**, 144427 (2009); D. Yamamoto, G. Marmorini, and I. Danshita, Microscopic Model Calculations for the Magnetization Process of Layered Triangular-Lattice Quantum Antiferromagnets, Phys. Rev. Lett. **114**, 027201 (2015).

[57] D. Lühmann, Cluster Gutzwiller method for bosonic lattice systems, Phys. Rev. A **87**, 043619 (2013).

[58] H. M. Deng, H. Dai, J. H. Huang, X. Z. Qin, J. Xu, H. H. Zhong, S. C. He, and C. H. Lee, Cluster Gutzwiller study of the Bose-Hubbard ladder: Ground-state phase diagram and many-body Landau-Zener dynamics, Phys. Rev. A **92**, 023618 (2015).

[59] M. Singh, S. Greschner, and M. Tapan, Anomalous pairing of bosons: Effect of multibody interactions in an optical lattice, Phys. Rev. A **98**, 023615 (2018).

[60] R. Suzuki and A. Koga, Cluster mean-field approach with density matrix renormalization group: Application to the hard-core bosonic Hubbard model on a triangular lattice, JPS Conf. Proc. **3**, 016005 (2014).

[61] D. Yamamoto, I. Danshita, and C. A. R. SadeMelo, Dipolar bosons in triangular optical lattices: Quantum phase transitions and anomalous hysteresis, Phys. Rev. A **85**, 021601(R) (2012).

[62] Y. C. Wang, W. Z. Zhang, H. Shao, and W. A. Guo, Extended Bose-Hubbard model with pair hopping on triangular lattice, Chin. Phys. B **22**, 96702 (2013).

[63] Y. C. Chen, R. G. Melko, S. Wessel, and Y. J. Kao, Supersolidity from defect condensation in the extended boson Hubbard model, Phys. Rev. B **77**, 014524 (2008).